The Cryosphere Discuss., 8, 21–53, 2014
www.the-cryosphere-discuss.net/8/21/2014/
doi:10.5194/tcd-8-21-2014

The Cryosphere Discussions
Open Access

Drifting snow measurements on the Greenland Ice Sheet and their application for model evaluation

J. T. M. Lenaerts[1], C. J. P. P. Smeets[1], K. Nishimura[2], M. Eijkelboom[1], W. Boot[1], M. R. van den Broeke[1], and W. J. van de Berg[1]

[1]Institute for Marine and Atmospheric Research Utrecht, Utrecht University, Utrecht, the Netherlands
[2]Graduate School of Environmental Studies, Nagoya University, Nagoya, Japan

Received: 18 December 2013 – Accepted: 19 December 2013 – Published: 6 January 2014

Correspondence to: J. T. M. Lenaerts (j.lenaerts@uu.nl)

Published by Copernicus Publications on behalf of the European Geosciences Union.

Abstract

This paper presents autonomous drifting snow observations performed on the Greenland Ice Sheet in the fall of 2012. High-frequency Snow Particle Counter (SPC) observations at ∼1 m above the surface provided drifting snow number fluxes and size distributions; these were combined with meteorological observations at six levels. We identify two types of drifting snow events: katabatic events are relatively cold and dry, with prevalent winds from the southeast, whereas synoptic events are short-lived, warm and wet. Precipitating snow during synoptic events disturbs the drifting snow measurements. Output of the regional atmospheric climate model RACMO2, which includes the drifting snow routine PIEKTUK-B, agrees well with the observed near-surface climate at the site, as well as with the frequency and timing of drifting snow events. Direct comparisons with the SPC observations at 1 m reveal that the model overestimates the typical size of drifting snow particles, as well as the horizontal snow transport at this level.

1 Introduction

The Greenland Ice Sheet (GrIS) has been losing mass in the recent two decades (Rignot et al., 2011; Shepherd et al., 2012) with further enhanced mass loss in recent warm years (Hanna et al., 2013). For the period 1992–2008, GrIS mass loss was equally distributed between increased calving from marine-terminating outlet glaciers and a rise in surface melt and subsequent runoff (Van den Broeke et al., 2009). However, large uncertainties remain in the quantification of the individual mass balance components and the temporal variability is large, obscuring an acceleration in the mass balance time series (Wouters et al., 2013). Particularly the surface mass balance (SMB), which is the sum of total mass gain (precipitation) and mass losses (surface sublimation (SU_s), drifting snow erosion (SU_{ds}), snow erosion (ER_{ds}) and surface runoff) at the ice sheet surface, is challenging to constrain in the absence of widespread, long-term observa-

TCD
8, 21–53, 2014

tions. Alternatively, regional climate models provide high-resolution gridded and multi-decadal estimates of SMB, and explicitly quantify individual SMB components (Ettema et al., 2009; Fettweis, 2007; Rae et al., 2012; Van Angelen et al., 2013). These models have indicated that the temporal and spatial variability of GrIS SMB is largely driven by precipitation and runoff, with snow sublimation and erosion one order of magnitude smaller (Lenaerts et al., 2012b). However, in the cold ice sheet interior, where katabatic forcing invokes strong and unidirectional winds throughout most of the year (Van Angelen et al., 2011), surface runoff is negligible and drifting snow sublimation and erosion are the only processes that remove mass from the surface. Drifting snow is known to enhance snow sublimation and locally to erode the surface snow layer, leading to a spatial redistribution of snow that is controlled by variations in the surface wind field. The frequency statistics of drifting snow are reasonably well documented, especially in Antarctica (Budd et al., 1966; Schmidt, 1982; Mann et al., 2000; Nishimura and Nemoto, 2005; Gallée et al., 2013) and for the seasonal snowcover in the Northern Hemisphere (Pomeroy et al., 1993; Déry and Yau, 2001); in general, however, the contribution of drifting snow sublimation and erosion to the SMB remains poorly constrained (Cierco et al., 2007). In recent years, Snow Particle Sensors (SPC), which have the ability to directly measure the horizontal snow transport and particle size spectrum, have been deployed in Antarctica (Gallée et al., 2013) and the Alps (Vionnet et al., 2012). In contrast, to date no extensive drifting snow measurements have been performed on the GrIS. Here we present results from autonomous, single-level SPC measurements collected in the lower accumulation area of western Greenland during fall 2012. These observations are complemented with high-frequency observations of vertical profiles of temperature, humidity and wind and autonomous imaging from automatic cameras. In this paper, we present the SPC measurements, discuss the feedback between drifting snow and climate, and apply these observations to evaluate the drifting snow characteristics simulated by the regional atmospheric climate model RACMO2 (Lenaerts et al., 2012b).

TCD
8, 21–53, 2014

2 Methods and data

2.1 Measurement location

A representative site for autonomous drifting snow observations should fulfill several criteria: frequent occurrence of drifting snow to quickly obtain a representative sample, low summer melt and modest accumulation rates for stability and to prevent burial of the installed equipment. Low-elevation areas of the GrIS are not suitable, as they are characterised by extensive summer melt, net ablation and limited occurrence of drifting snow (Lenaerts et al., 2012b). Better suited is the lower accumulation zone, where summer ablation and winter accumulation are modest, so that the experiment can be started at the end of the summer.

The site should be easily accessible by helicopter for deployment or recovery work, and have background climate information available. At the western margin of the GrIS, the Institute for Marine and Atmospheric Research of Utrecht University (UU/IMAU) has since 1997 operated Automatic Weather Stations (AWS) on the ice, close to the international airport of Kangerlussuaq (Fig. 1). For the drifting snow setup, we chose the highest station location (S10), located at an elevation of ~ 1850 m, approximately 300 m above the equilibrium line (Fig. 1, Van de Wal et al., 2012). The annual average temperature at S10 is around $-15\,^{\circ}$C (Fig. 2b), and melting occurs only during 3 months in summer (Fig. 2a). Average 10 m wind speed is $\sim 8\,\mathrm{m\,s^{-1}}$, with a winter maximum from a combined katabatic and synoptic forcing (Van Angelen et al., 2011) (Fig. 2b). RACMO2 results indicate that the drifting snow season at S10 extends over 9 months, when SU_{ds} is larger than both SU_s and runoff; only June, July and August have few drifting snow events due to melt-related compaction and wetting of the surface snow (Fig. 2a). In winter, SU_{ds} is estimated to remove $\sim 10\,\%$ of the precipitated snow.

TCD
8, 21–53, 2014

2.2 Measurements

The drifting snow measurements (Fig. 3) were performed by Snow Particle Counters (SPC, Sato et al., 1993), manufactured and tested in Japan, and previously used in experiments in the French Alps and Antarctica. The SPC has a self-steering wind vane and is equipped with a super-luminescent diode sensor (Sugiura et al., 2009), which acts as a constant light source during the measurement. When a drifting snow particle passes through the light beam, first the light energy that enters the upwind side decreases, and consequently the same occurs on the downwind side. These signals are converted to two successive electrical pulses, whose voltage is directly proportional to the size of the particle (Sato et al., 1993). Each signal is classified into one of 32 size classes ($\sim$ 40 to 500 µm). Furthermore, the SPC measures the number flux of the snow particles based on each particle's diameter class (Sugiura et al., 2009); hence, the integrated horizontal mass flux q [kg m^{-2} s^{-1}] of snow can be obtained using:

$$q = \sum_{c_\mathrm{d}=1}^{32} q_\mathrm{d} = \sum_{c_\mathrm{d}=1}^{32} n_\mathrm{d} \frac{4}{3} \pi \left(\frac{d}{2}\right)^3 \rho_i \quad (1)$$

with q_d the flux per diameter class, c_d representing the index of each of the 32 diameter classes with median diameter d [m], n_d the measured number flux, expressed here in number of particles per area per time [m^{-2} s^{-1}], and ρ_i the density of ice (= 917 g m^{-3}). This derivation explicitly assumes that the transported snow particles are fully rounded, a valid approximation in cold and windy regions (Guyomarc'h and Mérindol, 1998).

In our Greenland setup, the two SPC's were initially installed at 0.5 m and 1 m above the snow surface, to capture the vertical gradient of the mass flux. The SPC's were fixed to a horizontal frame that was connected to an electric motor (Fig. 3c), to enable vertical movement of the frame when snow accumulates below the instruments. The SPC's require much energy ($\sim$ 15 W), which was provided by two wind generators placed 3 and 4 m above the surface (Fig. 3a and b). To save energy, the SPC's were switched off at low wind speeds ($<$ 5 m s^{-1}), when drifting snow does not occur.

TCD
8, 21–53, 2014

The drifting snow setup is complemented by a 8 m high profile tower (Fig. 3d) for measuring atmospheric surface layer profiles at high frequency (10 Hz, Table 1) for eddy covariance analysis of atmospheric turbulent motions. Wind speed sensors at 6 different heights capture the vertical wind speed profile, and thermocouples measure fast temperature variations Moreover, at 5 m height, direct eddy covariance measurements were performed, including a sonic anemometer, a thermocouple and an open path H_2O/C_2O analyser sampled at 10 Hz (Table 1). The latter LiCor instrument measures fast humidity fluctuations to quantify the latent heat flux in and above the drifting snow layer. Data from the profile tower will be analysed in a forthcoming paper.

All instruments were installed on 13 August 2012, and checked two weeks after. Unfortunately, the lowest SPC had been malfunctioning since the start of the measurements, and could not be repaired on site. The SPC at 1 m height worked properly until the first week of October, when strong riming and high wind speeds led to its failure. The meteorological instruments fixed to the mast worked throughout the entire winter, until the equipment was removed in May 2013. This paper focuses on the period during which all instruments were in operation and with significant drifting snow events, i.e. 7 September–6 October 2012 (day of year 250–280).

Upon data retrieval, we performed a thorough check on the observations and performed corrections or omitted data wherever necessary. Among others, we have corrected wind directions to account for mast tilting and relative humidity is corrected for low temperatures (Reijmer and Oerlemans, 2002). All the measurements are resampled to half-hourly time resolution.

2.3 Regional climate model

The regional atmospheric climate model RACMO version 2.3 (RACMO2 hereafter) combines the High Resolution Limited Area Model (HIRLAM, Undén et al., 2002) dynamical core and the description of the physical processes of the Integrated Forecast System of the European Centre for Medium Range Forecasts (ECMWF cycle CY33r1, ECMWF-IFS, 2008) (van Wessem et al., 2013). It is specifically adapted for use in

TCD
8, 21–53, 2014

polar regions, with the inclusion of a snow model that calculates melt of snow and subsequent refreezing and runoff (Bougamont et al., 2005; Ettema et al., 2010), an albedo scheme that follows the temporal evolution of snow grain size (Kuipers Munneke et al., 2011), and, most importantly for this application, drifting snow physics (Lenaerts et al., 2010, 2012a). This drifting snow routine is based on the bulk blowing snow model PIEKTUK-B (Déry and Yau, 1999) and adapted to capture the interactions between drifting snow and the snow surface (based on Guyomarc'h and Mérindol, 1998) and the atmosphere (Lenaerts et al., 2012a). Earlier studies have shown good correspondence between observed and simulated drifting snow frequency and transport in Antarctica (Lenaerts et al., 2012a), and near-surface winds in Antarctica (Sanz Rodrigo et al., 2012) and Greenland (Ettema et al., 2010). Here we apply RACMO2 to the Greenland Ice Sheet at a horizontal resolution of ∼ 11 km, forced at its lateral boundaries and sea surface by ERA-Interim reanalysis fields (Dee et al., 2011). For this study we furthermore use RACMO2's ability to provide high temporal resolution output (6 min, resampled to 30 min) to enable a direct comparison with the observations. By default, PIEKTUK-B does not give information on the vertical profiles of snow transport; rather it assumes a certain vertical distribution and directly calculates the vertically integrated transport. To compare single-level measurements of snow transport with simulated snow transport, we retrieved detailed output of a stand-alone PIEKTUK-B model simulation, driven by atmospheric output of RACMO2 (for more details see Lenaerts et al., 2010).

3 Results

3.1 Near-surface climate

Figure 4 shows observed and simulated half-hourly average 2 m temperature, 10 m wind speed and 2 m relative humidity at S10. During the measurement campaign, 2 m temperature (Fig. 4a) varied from 250 K to the melting point. Cloud-free conditions were

TCD
8, 21–53, 2014

present during the first few days, indicated by the strong daily cycle in temperature and relatively low (katabatic) wind speeds (Fig. 4b). Around 10 September, a first synoptic system advected milder air, with temperatures close to the melting point, and high relative humidity and wind speed. Other synoptic disturbances brought similarly mild and windy conditions on 20 September, 26 September and 3 October, while drier conditions with katabatic winds prevailed in between. Figure 4 illustrates that RACMO2 is well able to simulate the temporal variability in temperature, wind speed and relative humidity. The correlation between RACMO2 and observations is significant, with a low mean model bias and a normalised RMSE $< 10\,\%$ for temperature, $\sim 20\,\%$ for wind speed and a larger bias and RMSE for relative humidity, which also inhibits a larger observational uncertainty (Table 1).

The observed snow height change in this period was ~ 40 cm, which is equivalent to ~ 120 mm w.e. of accumulation assuming a typical snow density of $\sim 300\,\mathrm{kg\,m^{-3}}$. The mass gain represents the sum of precipitation and deposition reduced by snow sublimation and erosion. For the same period, RACMO2 simulates 118 mm w.e. of precipitation, of which 0.5 mm fell as rain during the passage of a warm low-pressure system on 20 September (Fig. 4a). RACMO2 furthermore simulates a cumulative SU_{ds} of 12 mm w.e., with ER_{ds} an order of magnitude smaller < 1 mm w.e., yielding an SMB of ~ 106 mm w.e., which agrees within $\sim 15\,\%$ with the measured snow height change under the assumption that the accumulated snow has been compacted under relatively mild and windy conditions (Ligtenberg et al., 2011).

Supplement Movies 1 and 2 show the animated hourly camera snapshots during the period analysed here. The weather at S10 is typically characterised by two regimes: dry episodes with mixed synoptic/katabatic winds, mainly directed from the southeast, and intermittent, short-lived passages of low-pressure systems, bringing precipitation and strong southwesterly winds. This climate is clearly reflected in Fig. 5. Drifting snow occurs when the katabatic forcing is strong, with southeasterly winds, relatively low temperatures (~ 265 K) and relative humidities (80–90 %). Drifting snow events forced by synoptic intrusions from the southwest are characterised by higher tempera-

TCD
8, 21–53, 2014

tures (~ 270 K) and relative humidities (90–100 %). Figure 5b shows that during these events, similar snow transport fluxes are found along with lower wind speeds compared to katabatic events; since these events usually bring snowfall, it is likely that the SPC also measured precipitating snow along with drifting snow, the former having larger particle sizes. This is further demonstrated in Fig. 5d, which shows that the measured mean particle size during drifting snow is typically 100–200 µm, but rises to > 350 µm when winds are from southwest and drifting snow is likely accompanied by snowfall.

In RACMO2, drifting snow occurs when the threshold friction velocity is exceeded (Fig. 6a). The threshold value is a function of surface snow density (Lenaerts et al., 2012a), which in turn is determined by the relative amount of fresh snow in the upper model snow layer. The simulated friction velocity matches the observed friction velocity quite well (Fig. 6a); Fig. 6b shows that timing and frequency of simulated and observed drifting events also qualitatively agree, supporting that the parametrization of the threshold friction velocity in RACMO2, which is based on Antarctic snowdrift frequencies, is universally applicable. For instance, the warm drifting snow event on 20 September led to a small amount of liquid precipitation and melt of the snow surface, increasing surface snow density and the associated threshold friction velocity from 0.4 to 0.55 $m s^{-1}$. As a result, although actual friction velocities remained high during the remainder of the event, drifting snow remained limited to some short episodes, both in the model and in the observations (Fig. 6). Figure 6c demonstrates that during the strongest events, > 10^6 snow particles of each snow particle class 50–150 µm were detected. Generally, these snow particles are very small (< 150 µm), but the frequency of larger snow particles increases in the largest events, when vertical turbulent motions are sufficiently strong to lift up heavier particles from the surface, which are subsequently entrained in the drifting snow layer.

TCD
8, 21–53, 2014

4 Case studies

For a more detailed analysis of the drifting snow characteristics at S10 and the ability of RACMO2 to simulate these, we focus on two strong events, an event without snowfall that occurred on 24 September 2012, and a mixed snowfall and drifting snow event on 26 September 2012.

4.1 Dry event: 24 September 2012

On 24 September 2012, winds at S10 were from the southeast during the entire day (Fig. 7a). During the afternoon a low pressure area moved from south to north across Baffin Bay (Fig. 8), bringing precipitation at S10 and changing the wind direction to southerly in the evening. The automatic camera (Fig. 9) detected a clear start of the day, with low temperatures of $\sim -18\,^{\circ}\mathrm{C}$ (Fig. 7b), followed by a gradual rise in near-surface temperature, humidity and wind speed during the afternoon and evening. RACMO2 simulates drifting snow to start at 08:00 UTC (note that local time is UTC − 3 h), whereas the observations at 1 m detected the first drifting snow at 12:00 UTC; this appears to be related to an overestimation of friction velocity in RACMO2 (Fig. 7a). The good visibility in the image of 13:00 UTC and 16:00 UTC indicate that this was a small drifting snow event. However, movement of irregularities at the surface can be discerned between the two snapshots (Fig. 9), indicative of the occurrence of drifting snow. The camera images indicate that the skies were clear until 19:00 UTC, and first snowfall in RACMO2 only started around that time (Fig. 7c), so most of the drifting snow event was not associated with snowfall.

Particle size distributions in drifting snow models are usually parameterised by a two-parameter gamma distribution (Schmidt, 1982) with a shape parameter α constant with height. In PIEKTUK-B, α is assumed to be equal to 2, which has been estimated from observations in Antarctica close to the snow surface (Déry and Yau, 1999). Figure 10a shows the observed and simulated particle size distributions. The simulated particle sizes are underestimated by an approximate factor of two, if we use mean

TCD
8, 21–53, 2014

particle diameter ($\sim 100\,\mu m$ and $\sim 50\,\mu m$, respectively). This suggests that drifting snow particles are larger in Greenland than those typically observed on Antarctica (Nishimura and Nemoto, 2005; Yang and Yau, 2008). When a gamma distribution is fitted to the observed spectra, values of α range from 5 to 8.

Smaller snow particles are lighter, and therefore more easily suspended in the drifting snow layer. Therefore, larger amounts of drifting snow particles are simulated higher in the drifting snow layer in PIEKTUK-B than in the observations (Fig. 10b), and we find an overestimation of the simulated TR_{ds} of several orders of magnitude (Fig. 10c) at all temporal snapshots during the event of 24 September 2012. Accumulated over the day, PIEKTUK-B simulates the local snow horizontal transport at 1 m to be $\sim 210\,kg\,m^{-2}$, whereas the SPC measured around $\sim 1.5\,kg\,m^{-2}$ of cumulative snow transport at that height.

4.2 Mixed snowfall and drifting snow event: 26 September 2012

Here we focus on the strongest measured event during the campaign, occurring on 26 September 2012. Figure 11 shows the development of the large-scale synoptic situation during that day. In the early night (00:00–06:00 UTC), we see the strong (katabatic) southeasterly winds at S10. During the second part of the morning (06:00–12:00 UTC) a low-pressure system has developed that started to move northward along the coast, strengthening the katabatic winds with a synoptic component. This low-pressure system moved further northward in the afternoon, leading to a transient wind direction change from east to south at S10 (Fig. 12a). In the evening, the system moved north of S10 and decreased in strength (18:00–00:00 UTC). Our automatic camera made hourly snapshots of the event (Fig. 13), which show clear conditions in the morning with some drifting snow close to the surface (11:00 UTC), heavy drifting snow with low visibility at noon (15:00 UTC), and quieter conditions with overcast skies and high humidity in the afternoon (19:00 UTC).

RACMO2 simulates small drifting snow transport (TR_{ds}) during the earlier morning from 04:00 UTC onwards, increasing in the afternoon and ceasing in the evening

TCD
8, 21–53, 2014

(Fig. 11). Figure 12 shows that the SPC at 1 m started to detect drifting snow at 07:30 UTC. During the remainder of the morning, the drifting snow was probably confined to the saltation layer close to the surface, with marginal values at 1 m, which is confirmed by the webcam image of 11:00 UTC (Fig. 13). At 13:00 UTC, a sudden increase in TR_{ds} was observed, concurring with an increase in friction velocity from 0.55 m s^{-1} to 0.8 m s^{-1}. Along with an increase in TR_{ds}, RACMO2 simulates the onset of snowfall around this time (Fig. 12c), which likely contributed to the sudden increase in the detection of (mainly larger) snow particles (Fig. 12d). Also during this event, we see that the model overestimates the observed number fluxes and horizontal transport, although the model bias is smaller than in the katabatic case (Fig. 12). The single-level snow transport at 26 September is $\sim$ 335 kg m^{-2}, and the SPC measured $\sim$ 50 kg m^{-2}.

5 Conclusions

This paper presents the first detailed observations of drifting snow on the GrIS, performed during fall 2012 at site S10, located along the K-transect at $\sim$ 1850 m in the accumulation area of the western GrIS. During $\sim$ 30 days, a single-level SPC at 1 m above the snow surface continuously measured snow horizontal transport, complemented by high-frequency vertical profiles of atmospheric variables and hourly automatic camera images. At S10, drifting snow events occur during katabatic wind events, when winds are southeasterly and the near-surface atmosphere is dry and relatively cold. Alternatively, drifting snow events may occur at S10 during the passage of synoptic disturbances along the coast, characterised by southwesterly winds and often associated with precipitation and a warmer near-surface atmosphere.

This dataset of drifting snow observations is used to evaluate the regional atmospheric climate model RACMO2, which includes the PIEKTUK-B drifting snow model, in terms of its ability to simulate drifting snow characteristics. The model is well able to simulate the near-surface climate and to capture the majority of the observed drifting snow events. Two case studies of drifting snow events are discussed in more detail.

TCD
8, 21–53, 2014

The first event is mainly caused by katabatic winds, and the second event by the passage of a low-pressure system. Although the timing of these events is reasonably well estimated, our results indicate that the size of the drifting snow particles in RACMO2 is underestimated. In contrast to Antarctica, where typical drifting snow particle diameter is ∼ 40 µm, we find mean particle sizes on the order of ∼ 100 µm. This is likely related to differences in climate conditions, with the atmosphere over the Antarctic ice sheet being windier and colder, yielding smaller surface snow grains and suppressing snow metamorphism (Scambos et al., 2007; Lyapustin et al., 2009), and the type of precipitation, with a larger contribution of small-grain diamond dust in Antarctica (Walden et al., 2003).

As a result, drifting snow transport in RACMO2/PIEKTUK-B is significantly overestimated in the katabatic case, but less so during the synoptic event. This can have various reasons; (1) the better agreement between observed and simulated friction velocity in the synoptic case; (2) the synoptic case is associated with fresh snowfall contributing to the observed transport; the effect of larger (fresh) snow particles may compensate for the model flux overestimation; or (3) a more general model deficiency in properly simulating the characteristics of small drifting snow events such as on 24 September, when saltation is the dominant transport process and snow suspension is limited (Bintanja, 2000). Model evaluation in Antarctica and in Wyoming, northern USA (Yang and Yau, 2008) showed similarly high simulated particle concentrations in PIEKTUK-B.

Here we find that the shape parameter α of the gamma snow particle size distribution is much larger (5–8) in the observations than used in PIEKTUK-B, where α is assumed to be equal to 2 and constant with height. This suggests that α should be varying regionally (depending on climate) and vertically. In agreement with the results presented here, the observations pointed to a shape parameter α approaching 5 in Antarctica and close to 7 at $z = 1$ m at the Wyoming site. Yang and Yau (2008) proposed the introduction of a variable α that increases with height in PIEKTUK-B, which decreased the model bias of simulated particle concentrations in the upper drifting layer. However,

TCD
8, 21–53, 2014

the time-integrated TR_{ds} were not significantly altered by this model improvement. With only single-level observations, it remains unanswered how well the simulated vertical profiles of snow transport compare to reality; future observational studies of drifting snow in Greenland should therefore ideally include multiple-level SPC measurements, to study the variations of size distributions with height. If performed autonomously, the location of the campaign must be carefully selected; S10 along the K-transect appears to be a good candidate for such an experiment.

Supplementary material related to this article is available online at http://www.the-cryosphere-discuss.net/8/21/2014/tcd-8-21-2014-supplement.zip.

References

Bintanja, R.: Snowdrift suspension and atmospheric turbulence, Part 1: Theoretical background and model description, Bound.-Lay. Meteorol., 95, 343–368, 2000. 33

Bougamont, M., Bamber, J. L., and Greuell, W.: A surface mass balance model for the Greenland Ice Sheet, J. Geophys. Res., 110, F04018, doi:10.1029/2005JF000348, 2005. 27

Budd, W. F., Dingle, W. R. J., and Radok, U.: The Byrd Snowdrift Project: Outline and Basic Results, vol. 9 of Antarctic research series, AGU, 1966. 23

Cierco, F.-X., Naaim-Bouvet, F., and Bellot, H.: Acoustic sensors for snowdrift measurements: how should they be used for research purposes?, Cold. Reg. Sci. Technol., 49, 74–87, doi:10.1016/j.coldregions.2007.01.002, 2007. 23

Dee, D. P., Uppala, S. M., Simmons, A. J., Berrisford, P., Poli, P., Kobayashi, S., Andrae, U., Balmaseda, M. A., Balsamo, G., Bauer, P., Bechtold, P., Beljaars, A. C. M., van de Berg, L., Bidlot, J., Bormann, N., Delsol, C., Dragani, R., Fuentes, M., Geer, A. J., Haimberger, L., Healy, S. B., Hersbach, H., Hólm, E. V., Isaksen, L., Kållberg, P., Köhler, M., Matricardi, M., McNally, A. P., Monge-Sanz, B. M., Morcrette, J.-J., Park, B.-K., Peubey, C., de Rosnay, P., Tavolato, C., Thépaut, J.-N., and Vitart, F.: The ERA-interim reanalysis: configuration and performance of the data assimilation system, Q. J. Roy. Meteor. Soc., 137, 553–597, doi:10.1002/qj.828, 2011. 27

TCD
8, 21–53, 2014

Déry, S. J. and Yau, M. K.: A bulk blowing snow model, Bound.-Lay. Meteorol., 93, 237–251, 1999. 27, 30
Déry, S. J. and Yau, M. K.: Simulation of blowing snow in the Canadian Arctic using a double-moment model, Bound.-Lay. Meteorol., 99, 297–316, 2001. 23
ECMWF-IFS: Part IV: Physical Processes (CY33R1), Tech. Rep., European Centre for Medium-Range Weather Forecasts (ECMWF), Reading, UK, 2008. 26
Ettema, J., van den Broeke, M. R., Van Meijgaard, E., Van de Berg, W. J., Bamber, J. L., Box, J. E., and Bales, R. C.: Higher surface mass balance of the Greenland ice sheet revealed by high-resolution climate modeling, Geophys. Res. Lett., 36, L12501, doi:10.1029/2009GL038110, 2009. 23
Ettema, J., van den Broeke, M. R., van Meijgaard, E., van de Berg, W. J., Box, J. E., and Steffen, K.: Climate of the Greenland ice sheet using a high-resolution climate model – Part 1: Evaluation, The Cryosphere, 4, 511–527, doi:10.5194/tc-4-511-2010, 2010. 27
Fettweis, X.: Reconstruction of the 1979–2006 Greenland ice sheet surface mass balance using the regional climate model MAR, The Cryosphere, 1, 21–40, doi:10.5194/tc-1-21-2007, 2007. 23
Gallée, H., Trouvilliez, A., Agosta, C., Genthon, C., Favier, V., and Naaim-Bouvet, F.: Transport of snow by the wind: a comparison between observations in Adélie land, Antarctica, and simulations made with the regional climate model MAR, Bound.-Layer Meteor., 146, 133–147, doi:10.1007/s10546-012-9764-z, 2013. 23
Guyomarc'h, G. and Mérindol, L.: Validation of a forecasting application of blowing snow periods, Ann. Glaciol., 26, 138–143, 1998. 25, 27
Hanna, E., Navarro, F. J., Pattyn, F., Domingues, C. M., Fettweis, X., Ivins, E. R., Nicholls, R. J., Ritz, C., Smith, B., Tulaczyk, S., Whitehouse, P. L., and Zwally, H. J.: Ice-sheet mass balance and climate change, Nature, 498, 51–59, doi:10.1038/nature12238, 2013. 22
Kuipers Munneke, P., van den Broeke, M. R., Lenaerts, J. T. M., Flanner, M. G., Gardner, A., and van de Berg, W. J.: A new albedo scheme for use in climate models over the Antarctic ice sheet, J. Geophys. Res., 116, D05114, doi:10.1029/2010JD015113, 2011. 27
Lenaerts, J. T. M., van den Broeke, M. R., Déry, S. J., König-Langlo, G., Ettema, J., and Munneke, P. K.: Modelling snowdrift sublimation on an Antarctic ice shelf, The Cryosphere, 4, 179–190, doi:10.5194/tc-4-179-2010, 2010. 27
Lenaerts, J. T. M., van den Broeke, M. R., Déry, S. J., van Meijgaard, E., van de Berg, W. J., Palm, S. P., and Sanz Rodrigo, J.: Regional climate modeling of drifting

TCD
8, 21–53, 2014

snow in Antarctica, Part I: Methods and model evaluation, J. Geophys. Res., 117, D05108, doi:10.1029/2011JD016145, 2012a. 27, 29
Lenaerts, J. T. M., van den Broeke, M. R., van Angelen, J. H., van Meijgaard, E., and Déry, S. J.: Drifting snow climate of the Greenland ice sheet: a study with a regional climate model, The Cryosphere, 6, 891–899, doi:10.5194/tc-6-891-2012, 2012b. 23, 24, 41
Ligtenberg, S. R. M., Helsen, M. M., and van den Broeke, M. R.: An improved semi-empirical model for the densification of Antarctic firn, The Cryosphere, 5, 809–819, doi:10.5194/tc-5-809-2011, 2011. 28
Lyapustin, A., Tedesco, M., Wang, Y., Aoki, T., Hori, M., and Kokhanovsky, A.: Retrieval of snow grain size over Greenland from MODIS, Remote Sens. Environ., 113, 1976–1987, doi:10.1016/j.rse.2009.05.008, 2009. 33
Mann, G. W., Anderson, P. S., and Mobbs, S. D.: Profile measurements of blowing snow at Halley, Antarctica, J. Geophys. Res., 105, 24491–24508, doi:10.1029/2000JD900247, 2000. 23
Nishimura, K. and Nemoto, M.: Blowing snow at Mizuho station, Antarctica, Philos. T. Roy. Soc. A, 363, 1647–1662, 2005. 23, 31
Pomeroy, J., Gray, D., and Landine, P.: The Prairie Blowing Snow Model: characteristics, validation, operation, J. Hydrol., 144, 165–192, doi:10.1016/0022-1694(93)90171-5, 1993. 23
Rae, J. G. L., Aðalgeirsdóttir, G., Edwards, T. L., Fettweis, X., Gregory, J. M., Hewitt, H. T., Lowe, J. A., Lucas-Picher, P., Mottram, R. H., Payne, A. J., Ridley, J. K., Shannon, S. R., van de Berg, W. J., van de Wal, R. S. W., and van den Broeke, M. R.: Greenland ice sheet surface mass balance: evaluating simulations and making projections with regional climate models, The Cryosphere, 6, 1275–1294, doi:10.5194/tc-6-1275-2012, 2012. 23
Reijmer, C. and Oerlemans, J.: Temporal and spatial variability of the surface energy balance in Dronning Maud Land, Antarctica, J. Geophys. Res., 107, 4759–4770, 2002. 26
Rignot, E., Velicogna, I., van den Broeke, M. R., Monaghan, A., and Lenaerts, J. T. M.: Acceleration of the contribution of Greenland and Antarctic ice sheets to sea level rise, Geophys. Res. Lett., 38, L05503, doi:10.1029/2011GL046583, 2011. 22
Sanz Rodrigo, J., Buchlin, J.-M., van Beeck, J., Lenaerts, J. T. M., and van den Broeke, M. R.: Evaluation of the Antarctic surface wind climate from ERA reanalyses and RACMO2/ANT simulations based on Automatic Weather Stations, Clim. Dynam., 1–24, doi:10.1007/s00382-012-1396-y, 2012. 27

TCD
8, 21–53, 2014

Sato, T., Kimura, T., Ishimaru, T., and Maruyama, T.: Field test of a new snow-particle counter (SPC) system, Ann. Glaciol., 18, 149–154, 1993. 25

Scambos, T., Haran, T., Fahnestock, M., Painter, T., and Bohlander, J.: MODIS-based Mosaic of Antarctica (MOA) data sets: continent-wide surface morphology and snow grain size, Remote Sens. Environ., 111, 242–257, doi:10.1016/j.rse.2006.12.020, 2007. 33

Schmidt, R.: Vertical profiles of wind speed, snow concentration and humidity in blowing snow, Bound.-Layer Meteor., 223–246, 1982. 23, 30

Shepherd, A., Ivins, E. R., A, G., Barletta, V. R., Bentley, M. J., Bettadpur, S., Briggs, K. H., Bromwich, D. H., Forsberg, R., Galin, N., Horwath, M., Jacobs, S., Joughin, I., King, M. A., Lenaerts, J. T. M., Li, J., Ligtenberg, S. R. M., Luckman, A., Luthcke, S. B., McMillan, M., Meister, R., Milne, G., Mouginot, J., Muir, A., Nicolas, J. P., Paden, J., Payne, A. J., Pritchard, H., Rignot, E., Rott, H., Sörensen, L. S., Scambos, T. A., Scheuchl, B., Schrama, E. J. O., Smith, B., Sundal, A. V., van Angelen, J. H., van de Berg, W. J., van den Broeke, M. R., Vaughan, D. G., Velicogna, I., Wahr, J., Whitehouse, P. L., Wingham, D. J., Yi, D., Young, D., and Zwally, H. J.: A reconciled estimate of ice-sheet mass balance, Science, 338, 1183–1189, doi:10.1126/science.1228102, 2012. 22

Sugiura, K., Ohata, T., Yang, D., Sato, T., and Sato, A.: Application of a snow particle counter to solid precipitation measurements under Arctic conditions, Cold. Reg. Sci. Technol., 58, 77–83, doi:10.1016/j.coldregions.2009.03.010, 2009. 25

Undén, P., Rontu, L., Järvinen, H., Lynch, P., Calvo, J., Cats, G., Cuxart, J., Eerola, K., Fortelius, C., Garcia-Moya, J., Jones, C., Lenderlink, G., McDonald, A., McGrath, R., Navascues, B., Nielsen, N. W., Ødegaard, V., Rodriguez, E., Rummukainen, M., Rööm, R., Sattler, K., Sass, B. H., Savijärvi, H., Schreur, B. W., Sigg, R., The, H., and Tijm, A.: HIRLAM-5 Scientific Documentation, Tech. Rep., Swed. Meteorol., and Hydrol. Inst., Norrköping, Sweden, 2002. 26

Van Angelen, J. H., van den Broeke, M. R., and van de Berg, W. J.: Momentum budget of the atmospheric boundary layer over the Greenland ice sheet and its surrounding seas, J. Geophys. Res.-Atmos., 116, D10101, doi:10.1029/2010JD015485, 2011. 23, 24

Van Angelen, J. H., Broeke, M. R., Wouters, B., and Lenaerts, J. T. M.: Contemporary (1960–2012) Evolution of the Climate and Surface Mass Balance of the Greenland Ice Sheet, Surv. Geophys., 1–20, doi:10.1007/s10712-013-9261-z, 2013. 23

TCD
8, 21–53, 2014

van de Wal, R. S. W., Boot, W., Smeets, C. J. P. P., Snellen, H., van den Broeke, M. R., and Oerlemans, J.: Twenty-one years of mass balance observations along the K-transect, West Greenland, Earth Syst. Sci. Data, 4, 31–35, doi:10.5194/essd-4-31-2012, 2012. 24

Van den Broeke, M. R., Bamber, J. L., Ettema, J., Rignot, E., Schrama, E., van de Berg, W. J., van Meijgaard, E., Velicogna, I., and Wouters, B.: Partitioning recent Greenland mass loss, Science, 326, 984–986, doi:10.1126/science.1178176, 2009. 22

Vionnet, V., Guyomarch, G., Bouvet, F. N., Martin, E., Durand, Y., Bellot, H., Bel, C., and Puglise, P.: Occurrence of blowing snow events at an alpine site over a 10-year period: observations and modelling, Adv. Water Resour., 55, 53–63, doi:10.1016/j.advwatres.2012.05.004, 2012. 23

Walden, V. P., Warren, S. G., and Tuttle, E.: Atmospheric ice crystals over the Antarctic Plateau in winter, J. Appl. Meteorol., 42, 1391–1405, doi:10.1175/1520-0450(2003)042<1391:AICOTA>2.0.CO;2, 2003. 33

Wouters, B., Bamber, J. L., van den Broeke, M. R., Lenaerts, J. T. M., and Sasgen, I.: Limits in detecting acceleration of ice sheet mass loss due to climate variability, Nat. Geosci., 6, 613–616, doi:10.1038/ngeo1874, 2013. 22

Yang, J. and Yau, M.: A new triple-moment blowing snow model, Bound.-Lay. Meteorol., 126, 137–155, doi:10.1007/s10546-007-9215-4, 2008. 31, 33

TCD
8, 21–53, 2014

Table 1. A list of all meteorological and turbulence instruments (sensors marked with [a] are manufactured by Campbell Scientific, Inc.).

variable	snow observations	accuracy	height (m)
snow transport	SPC, Niigata Electric	unknown	0.5, 1
snow height	SR50[a]	±0.01 m	/
variable	profile observations	accuracy	
u	05103-L R.M. Young	$\pm 0.3\,\mathrm{m\,s^{-1}}$	0.5, 1, 1.5, 2.5, 4, 8
dd	05103-L R.M. Young	±3 °C	0.5, 1, 1.5, 2.5, 4, 8
T	Vaisala HMP155	±0.4 °C at −20 °C	0.5, 1, 2.5, 4, 8
RH	Vaisala HMP155	±2 % (RH < 90 %)	0.5, 1, 2.5, 4, 8
T	FW3 Type E thermocouple[a]	±0.2 °C	0.5, 1, 1.5, 2.5, 4, 8
variable	turbulence observations	accuracy	
u, v, w	CSAT3 Sonic Anemometer[a]	offset error $< \pm 0.04\,\mathrm{m\,s^{-1}}$	5
T_{sonic}	CSAT3 Sonic Anemometer[a]	resolution ±0.025 °C	5
T	FW3 Type E thermocouple[a]	±0.2 °C	5
q	LI-COR LI-7500	RMS noise $< 0.005\,\mathrm{g\,kg^{-1}}$	5

TCD
8, 21–53, 2014

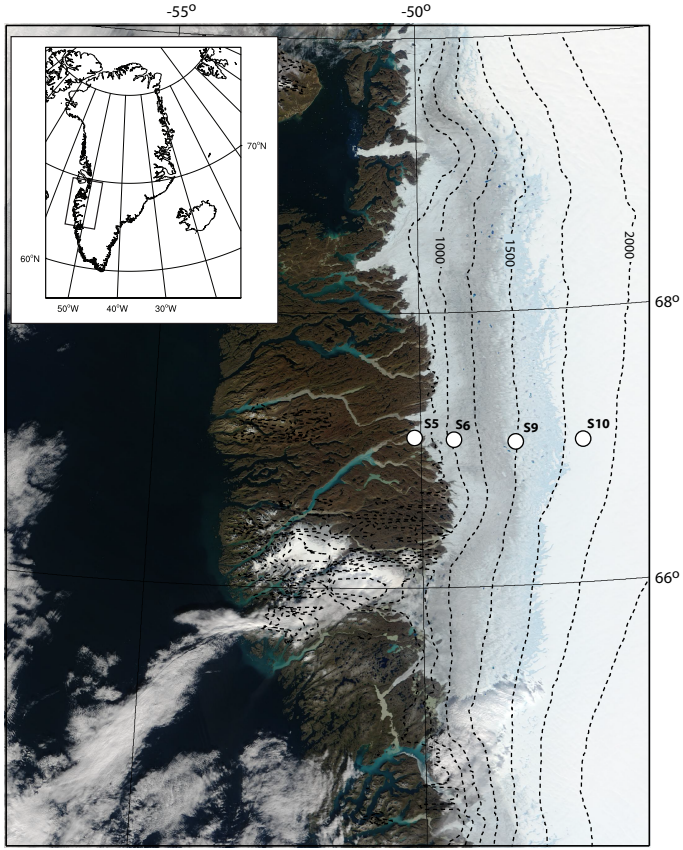

Fig. 1. Map of the location of the K-transect with stations S5, S6, S9 and S10. Background shows MODIS satellite image of August 2006. The inset locates the region on the Greenland ice sheet.

TCD
8, 21–53, 2014

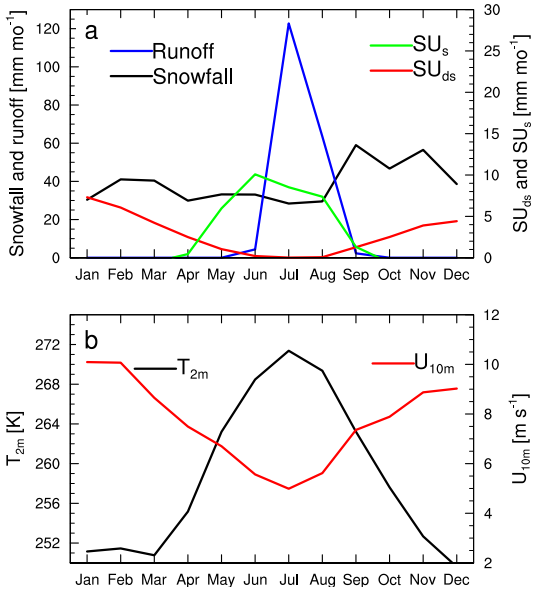

Fig. 2. Seasonal variability of **(a)** SMB components and **(b)** 2 m temperatures and 10 m wind speed at S10, according to RACMO2 (mean of 1960–2011, Lenaerts et al., 2012b). The left axis in **(a)** shows snowfall and runoff, the right axis shows drifting snow sublimation (SU_{ds}) and surface sublimation (SU_s). All are in mm month^{-1}. Note the different scales of left and right axes.

TCD
8, 21–53, 2014

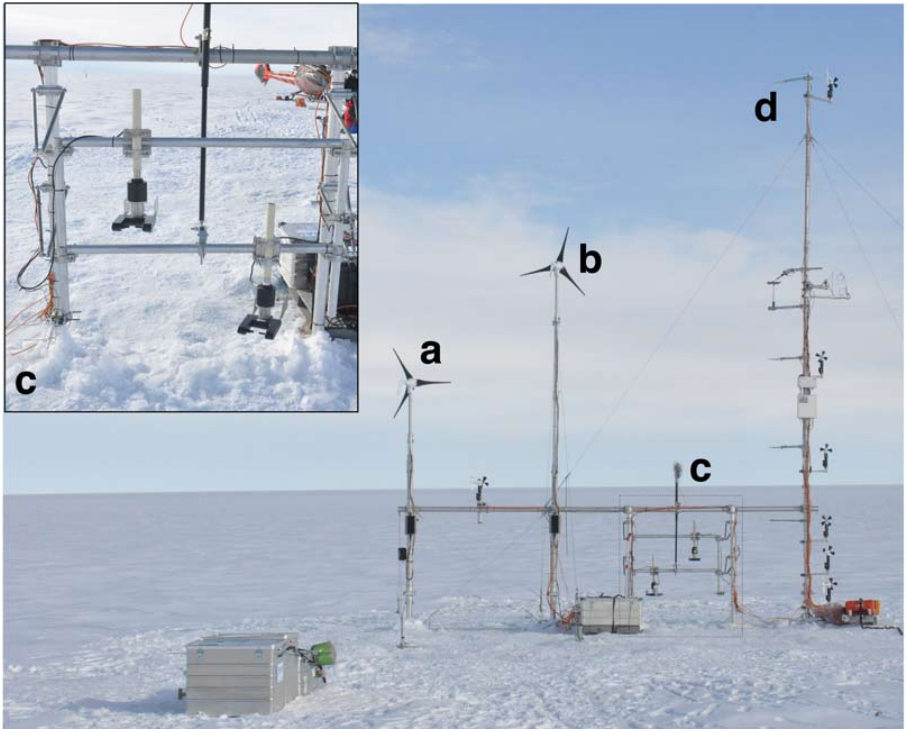

Fig. 3. Drifting snow equipment. Picture taken on 13 August 2012.

TCD
8, 21–53, 2014

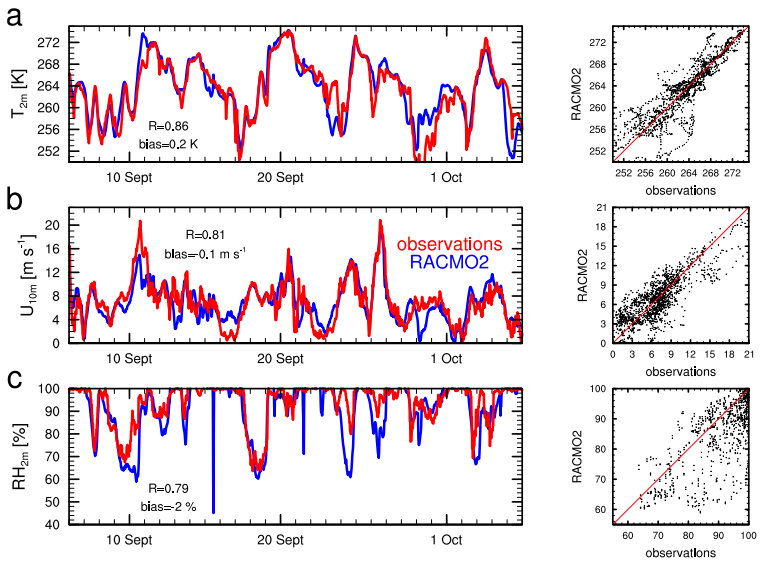

Fig. 4. Time evolution of **(a)** 2 m temperature, **(b)** 10 m wind speed and **(c)** relative humidity according to the observations (red lines) and RACMO2 (blue lines). The panels on the right show the correlations between observations and RACMO2, with the 1 : 1 line in red. The correlation coefficient (R) and mean bias are shown in the left panels.

TCD
8, 21–53, 2014

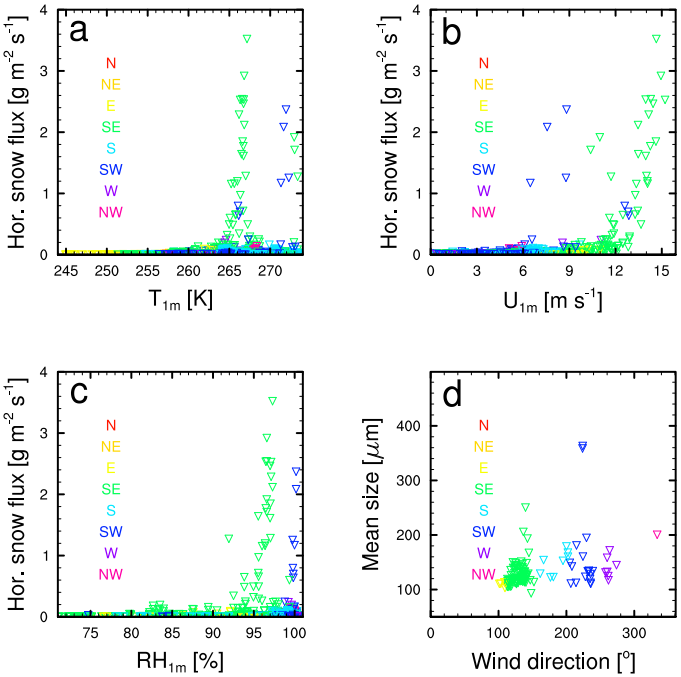

Fig. 5. Horizontal snow flux [g m^{-2} s^{-1}] vs. **(a)** temperature **(b)** wind speed and **(c)** relative humidity, all measured at ~ 1 m above the snow surface. **(d)** Mean snow particle size as a function of wind direction.

TCD
8, 21–53, 2014

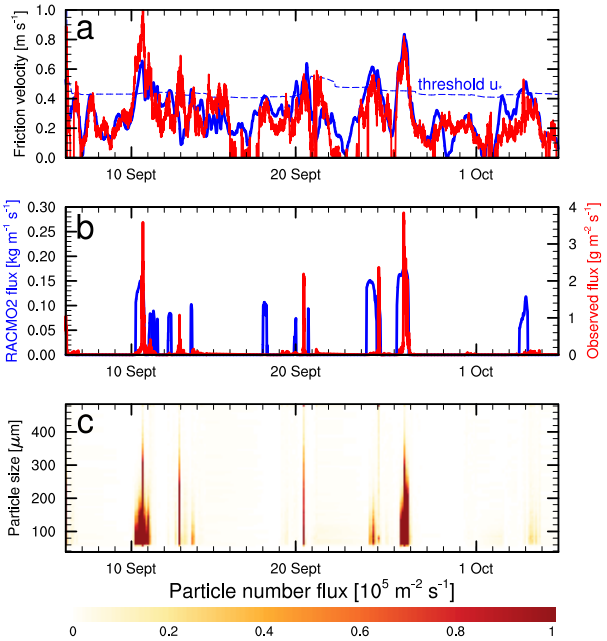

Fig. 6. Time evolution of **(a)** observed (red) and simulated friction velocity (blue), and threshold friction velocity for drifting snow in RACMO2 (dashed) blue); **(b)** observed (red) and simulated (blue) drifting snow transport, with the observations originating from 1 level only, whereas RACMO2 snow transport is vertically integrated (mind the different units); and **(c)** observed number of snow particles per particle size.

TCD
8, 21–53, 2014

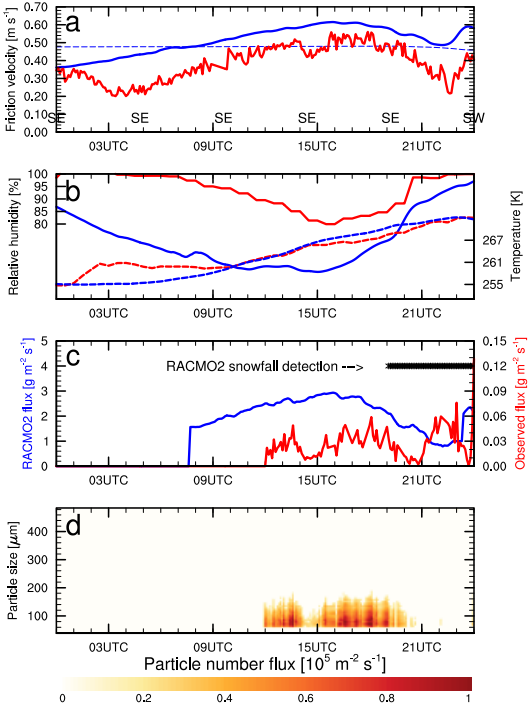

Fig. 7. Time evolution on 24 September 2012 of **(a)** observed (red) and simulated friction velocity (blue) and wind direction (indicated above bottom axis), and threshold friction velocity for drifting snow in RACMO2 (dashed blue); **(b)** observed (red) and simulated (blue) relative humidity (solid) and temperature (dashed) at ~ 1 m above the surface; **(c)** observed (red) and simulated (blue) single-level (1 m) drifting snow transport (mind the different scales); and **(d)** observed number of snow particles per particle size. The crosses in **(c)** indicate the occurrence of snowfall in RACMO2.

TCD
8, 21–53, 2014

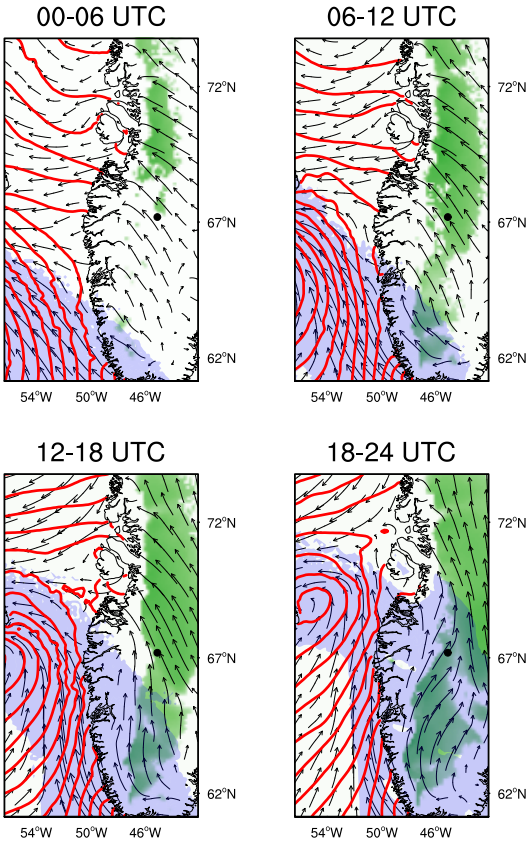

Fig. 8. Time evolution of the large-scale weather situation on 24 September 2012, with sea-level pressure (red lines), 10 m wind (black arrows), precipitation (shaded blue if > 1 mm w.e. per 6 h) and drifting snow transport (shaded green if > 6000 kg m^{-1} per 6 h). The location of S10 is indicated by the black dot in each panel.

TCD
8, 21–53, 2014

Fig. 9. Automatic camera images of the measurement system on 26 September at 11:00 UTC, 15:00 UTC and 19:00 UTC. The automatic camera was positioned ~ 10 m away of the instrumental setup.

TCD
8, 21–53, 2014

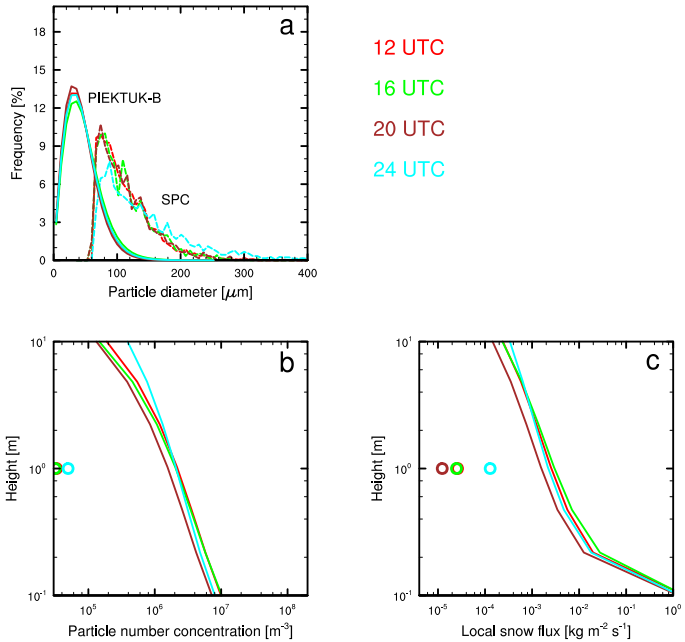

Fig. 10. Snapshots of drifting snow characteristics during 24 September 2012. **(a)** Relative frequency of drifting snow particle sizes at 1 m above the surface according to PIEKTUK-B (solid lines) and observations (dotted lines); **(b)** and **(c)** vertical profiles of simulated particle concentration and horizontal snow flux (solid lines) and observed particle concentration and horizontal snow flux at ~ 1 height (filled dots).

TCD
8, 21–53, 2014

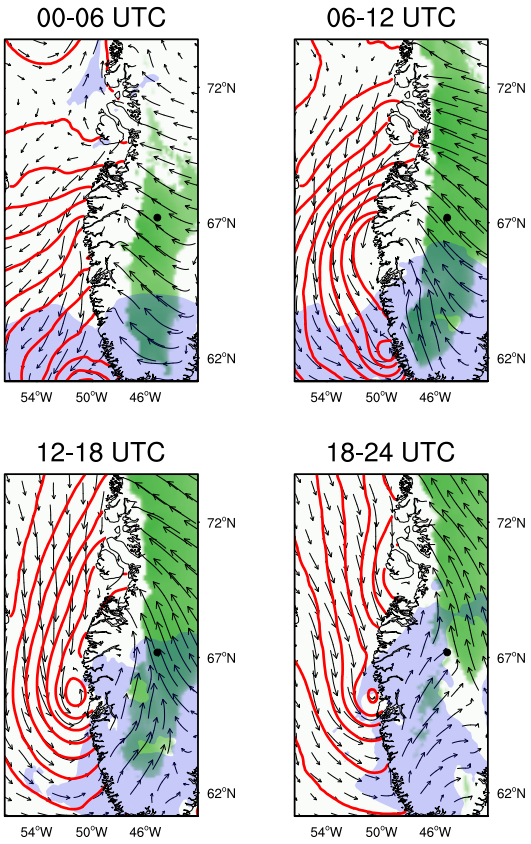

Fig. 11. Time evolution of the large-scale weather situation on 26 September 2012, with sea-level pressure (red lines), 10 m wind (black arrows), precipitation (shaded blue if > 1 mm w.e. per 6 h) and drifting snow transport (shaded green if > 6000 kg m^{-1} per 6 h). The location of S10 is indicated by the black dot in each panel.

TCD
8, 21–53, 2014

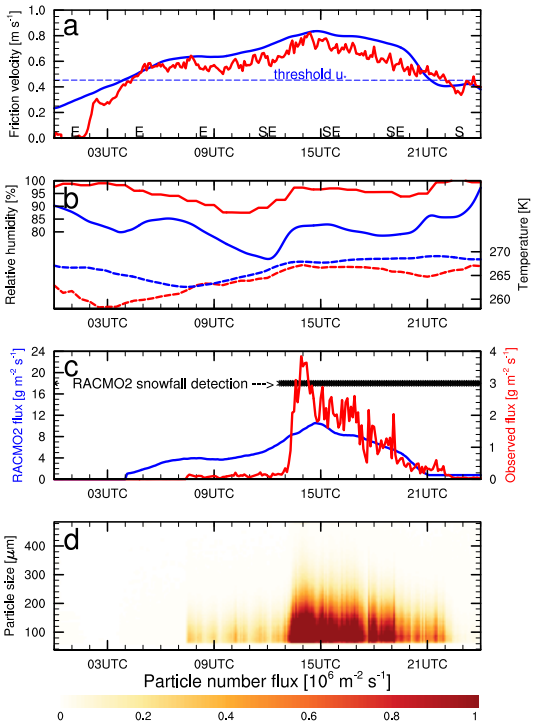

Fig. 12. Time evolution on 26 September 2012 of **(a)** observed (red) and simulated friction velocity (blue) and wind direction (indicated above bottom axis), and threshold friction velocity for drifting snow in RACMO2 (dashed blue); **(b)** observed (red) and simulated (blue) relative humidity (solid) and temperature (dashed) at ~ 1 m above the surface; **(c)** observed (red) and simulated (blue) drifting snow transport, with the observations originating from 1 level only, whereas RACMO2 snow transport is vertically integrated (mind the different units); and **(d)** observed number of snow particles per particle size. The crosses in **(c)** indicate the occurrence of snowfall in RACMO2. Note that the labelbar legend in **(d)** is increased by a factor of 10 compared to Fig. 6.

TCD
8, 21–53, 2014

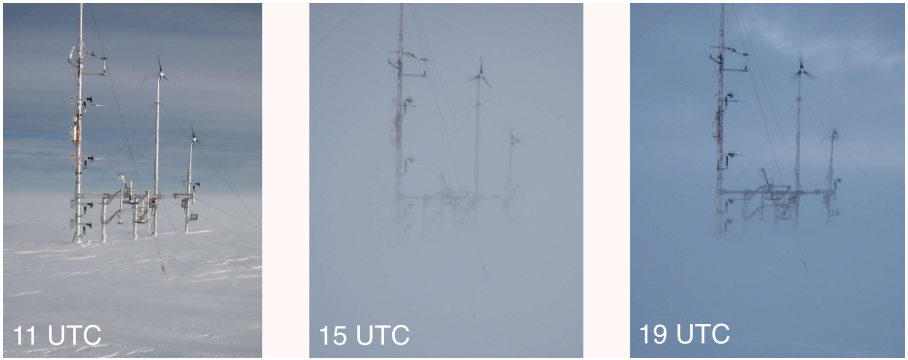

Fig. 13. Automatic camera images of the measurement system on 26 September at 11:00 UTC, 15:00 UTC and 19:00 UTC. The automatic camera was positioned ~ 10 m away of the instrumental setup.

TCD
8, 21–53, 2014

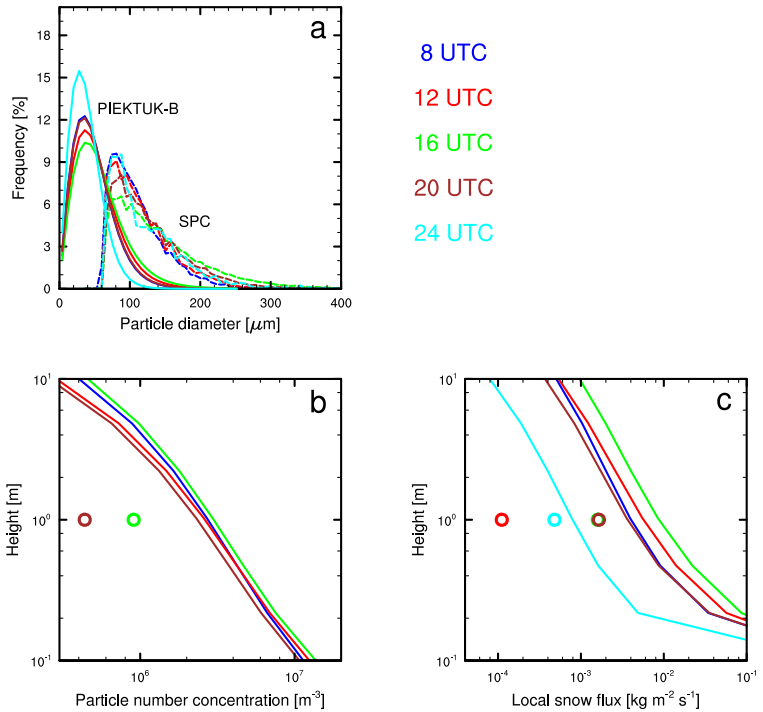

Fig. 14. Snapshots of drifting snow characteristics during 26 September 2012. **(a)** Relative frequency of drifting snow particle sizes at 1 m above the surface according to PIEKTUK-B (solid lines) and observations (dotted lines); **(b)** and **(c)** vertical profiles of simulated particle concentration and horizontal snow flux (solid lines) and observed particle concentration and horizontal snow flux at ~ 1 height (filled dots).

TCD
8, 21–53, 2014